Characterization of the primary radical pair in reaction centers of heliobacillus mobilis by 13C Photo-CIDNP MAS NMR

Roy, E.; Rohmer, T.; Gast, P.; Jeschke, G.; Alia, A.; Matysik, J.

Characterization of the Primary Radical Pair in Reaction Centers of *Heliobacillus mobilis* by ^{13}C Photo-CIDNP MAS NMR†

Esha Roy,‡ Thierry Rohmer,‡ Peter Gast,§ Gunnar Jeschke,|| A. Alia,‡ and Jörg Matysik*,‡

Leiden Institute of Chemistry, P.O. Box 9502, 2300 RA Leiden, The Netherlands, Leiden Institute of Physics, P.O. box 9504, 2300 RA Leiden, The Netherlands, and Physikalische Chemie, Universität Konstanz, 78457 Konstanz, Germany

Received January 7, 2008; Revised Manuscript Received February 13, 2008

ABSTRACT: Photochemically induced dynamic nuclear polarization (photo-CIDNP) has been observed in membrane fragments of heliobacterium *Heliobacillus mobilis* without further isolation by ^{13}C magic-angle spinning (MAS) solid-state NMR under continuous illumination with white light. In the ^{13}C photo-CIDNP MAS NMR spectra of heliobacterial membrane fragments, two sets of signals are observed, allowing characterization of the primary radical pair. One set, showing enhanced absorptive (positive) signals, arises from the BChl *g* donor, while the set of emissive (negative) signals is assigned to the 8^1-hydroxy Chl *a* acceptor. Hence, under these sample conditions, both donor and acceptor sides are either monomeric or composed of identical cofactors. The occurrence of the differential relaxation (DR) mechanism suggests a donor triplet lifetime in the microsecond range. It appears that the occurrence of the solid-state photo-CIDNP effect is a general feature of primary radical pairs in natural photosynthesis.

In heliobacteria, antenna pigments and the RC[1] are bound to a single pigment–protein complex embedded in the cytoplasmic membrane (for reviews, see refs *1–3*). Heliobacterial RCs are characterized by the presence of a bacteriochlorophyll *g* (BChl *g*) cofactor (Figure 1A) (*4–6*). The primary electron donor in the RC is termed either P798 (*7*) or P800 (*8*) and has been reported to be a dimer comprising either two BChl *g* cofactors (*9*) or both the 13^2-epimers BChl *g* and BChl *g*′ (*10*). ENDOR studies indicate that in the primary electron donor the unpaired electron is symmetrically delocalized over the two dimer halves (*11*), and FTIR data indicate that the positive charge is shared between two coupled BChl cofactors (*12*). Spectroscopic information and chemical analysis established the structure to be 8^1-hydroxy-Chl *a* esterified with a farnesol side chain (Figure 1B) (*13*). The pigment composition per RC is 35–40 molecules of BChl *g* (*2*), two molecules of BChl *g*′ (*10*), two molecules of 8^1-hydroxy-Chl *a* (*13*), and approximately two to three carotenoid molecules (*1, 14*). Membranes of heliobacteria contain menaquinone in the RC (*15*), but there is no clear evidence establishing its role as an intermediate in the forward electron transfer (*1*). EPR and optical spectroscopic data indicate the presence of an iron−sulfur center similar to F_x in PSI (*9, 16, 17*) acting as an electron acceptor, and recently, the presence of F_A and F_B clusters has been reported (*18*).

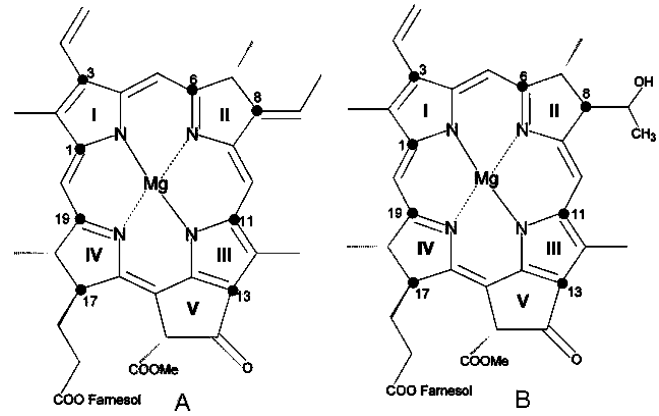

FIGURE 1: Structure of 4-ALA ^{13}C-labeled BChl *g* (A) and 8^1-hydroxy-Chl *a* (B) molecules. The ^{13}C label positions are indicated by filled circles (●). Numbering is according to IUPAC nomenclature.

The solid-state photo-CIDNP (photochemically induced dynamic nuclear polarization) effect has been observed for the first time in quinone-blocked frozen samples of RCs of *Rhodobacter* (*Rb.*) *sphaeroides* R26 under illumination by ^{15}N magic-angle spinning (MAS) solid-state NMR (*19*). Until now, the observation of the solid-state photo-CIDNP effect (for reviews, see refs *20* and *21*) is limited to natural photosynthetic RCs. The effect has been observed by MAS NMR in purple bacterial RCs from *Rb. sphaeroides* R26 and wild type (WT) (*22, 23*), in plant photosystem (PS) I and II (*24–27*), and recently in RCs from green sulfur bacterium *Chlorobium* (*C.*) *tepidum* (*28*). In addition, NMR signals

† This work has been financially supported by The Netherlands Organization for Scientific Research (NWO) through Jonge Chemici award (700.50.521) and a Vidi grant (700.53.423) as well as by the Volkswagen-Stiftung (I/78010) to J.M.

* To whom correspondence should be addressed. Telephone: +31-71-5274198. Fax: +31-71-5274603. E-mail: j.matysik@chem.leidenuniv.nl.

‡ Leiden Institute of Chemistry.

§ Leiden Institute of Physics.

|| Universität Konstanz.

[1] Abbreviations: ALA, Δ-aminolevulinic acid; (B)Chl, (bacterio)chlorophyll; DD, differential decay; DR, differential relaxation; ENDOR, electron–nuclear double resonance; FTIR, Fourier transform infrared; NMR, nuclear magnetic resonance; MAS, magic-angle spinning; photo-CIDNP, photo-chemically induced dynamic nuclear polarization; PSI, photosystem I; PSII, photosystem II; RC, reaction center; TSM, electron–electron−nuclear three-spin mixing; WT, wild type.

10.1021/bi800030g CCC: $40.75
Published on Web 03/28/2008

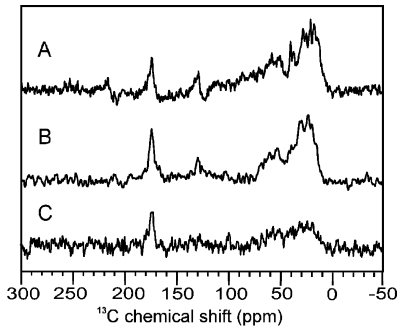

FIGURE 2: ^{13}C MAS NMR spectra of natural abundance membrane fragments of *Hba. mobilis* obtained in the dark at 17.6 (A), 9.4 (B), and 4.7 T (C), using a MAS frequency of 8 kHz.

were detected in entire membrane-bound photosynthetic units (*29*) and whole cells (*23*) of *Rb. sphaeroides*. Hence, the question arises of whether photo-CIDNP is an intrinsic property of light-induced electron transfer in natural RCs.

The origin of photo-CIDNP observed in the solid state in photosynthetic RCs is explained by occurrence of three mechanisms (*20, 22, 23*). The three-spin mixing (TSM) mechanism (*30*) depends on the coupling between two electron spins in a radical pair, leading to enhanced electron polarization of the cofactors involved, which is transferred by anisotropic hyperfine coupling into polarization of nuclear spins. The differential decay (DD) mechanism (*31*) requires different lifetimes of the singlet and triplet states. The third mechanism is active in systems having a long-lived triplet state of the donor, which leads to the differential relaxation (DR) between the nuclear spins in the triplet and singlet ground state of the special pair (*32*). All mechanisms lead to *net* nuclear polarization by unbalancing the two decay channels of the radical pair which leads to an excess of either α or β nuclear spins. This enhanced nuclear polarization is generated on the time scale of seconds and can be detected by MAS NMR. Chemical shifts observed by photo-CIDNP MAS NMR provide information about the electronic ground-state structures of the electron donor and acceptor forming a correlated radical pair. In addition, photo-CIDNP MAS NMR intensities are related to the local electron spin densities in the electron donor and the electron acceptor during the radical pair state. Selective ^{13}C isotope labeling at numerous cofactor positions in bacterial RCs provided the study of the ground-state electronic structure of the special pair (*33, 34*). Here, we analyze the spin-chemical machinery of RCs of *Heliobacillus mobilis*, using ^{13}C photo-CIDNP MAS NMR.

MATERIALS AND METHODS

Sample Preparation. Hba. mobilis cells were grown as described by van de Meent et al. (*35*). The cells were harvested after a period of 7 days by centrifugation and resuspended in a buffer containing 20 mM Tris-HCl and 10 mM sodium ascorbate (pH 8.0). The membrane fragments were prepared by sonication of the cells for 35 min followed by a 15 min centrifugation at 40000*g*. The resulting supernatant was ultracentrifuged for 2 h at 200000*g* and 4 °C. The pellet containing the membrane fragments was resuspended in 50 mM glycine buffer with 0.02% SB-12 (pH 10.8). For photo-CIDNP studies, the sample was reduced by 50 mM sodium dithionite.

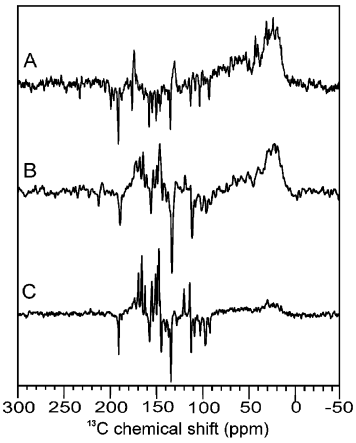

FIGURE 3: ^{13}C photo-CIDNP MAS NMR spectra of natural abundance membrane fragments of *Hba. mobilis* obtained under continuous illumination at 17.6 (A), 9.4 (B), and 4.7 T (C), using a MAS frequency of 8 kHz. Artificial line broadening of 120, 50, and 30 Hz is used in spectra A−C, respectively.

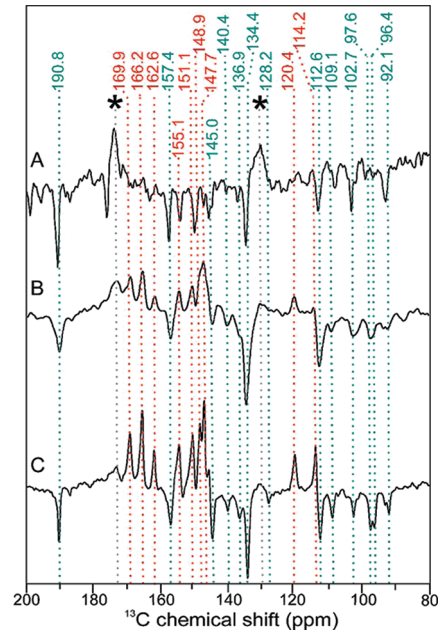

FIGURE 4: Detailed view of the region showing ^{13}C photo-CIDNP MAS NMR spectra of natural abundance membrane fragments obtained under continuous illumination at a MAS frequency of 8 kHz at 17.6 (A), 9.4 (B), and 4.7 T (C). Centerbands are shown as dashed lines. Signals labeled with an asterisk originate from the protein and are not light-induced. The positive signals are labeled in red, while the negative signals are labeled in green.

Preparation of Selective ^{13}C-Labeled Membrane Fragments. Selective isotope enrichment of (bacterio)chlorophylls in *Hba. mobilis* was achieved by growing bacterial cultures anaerobically in the presence of 1.0 mM [4-^{13}C]-δ-aminolevulinic acid (ALA) ([4-^{13}C]$COOHCH_2CH_2{}^{13}COCH_2NH_2 \cdot HCl$, 99% ^{13}C-enriched) purchased from Cambridge Isotope Laboratories (Andover, MA). The incorporation of [4-^{13}C]ALA produces (bacterio)chlorophylls labeled at C-1, C-3, C-6, C-8, C-11, C-13, C-17, and C-19 (Figure 1). The preparation of isolated membranes was carried out as described above. For measurement of the ^{13}C isotope label concentration, see the Supporting Information.

MAS NMR Measurements. The NMR experiments were performed at different magnetic fields using AV-750, DMX-400, and DMX-200 NMR spectrometers (Bruker-Biospin

GmbH, Karlsruhe, Germany). The samples were loaded into optically transparent 4 mm sapphire rotors. All experiments were performed at 233 K. The illumination setup used has been specially designed for a Bruker MAS probe (*21*). The light and dark spectra were obtained with a Hahn-echo pulse sequence and two-pulse phase modulation proton decoupling. If not stated differently, the cycle delay was 4 s and the MAS frequency 8 kHz. All spectra were externally referenced to the ^{13}COOH response of solid tyrosine HCl at 172.1 ppm.

RESULTS AND DISCUSSION

Field Dependence of the Photo-CIDNP Effect. The ^{13}C MAS NMR spectra obtained from natural abundance samples of *Hba. mobilis* membrane fragments in the dark (Figure 2) exhibit features characteristic of a ^{13}C MAS NMR spectrum of a protein, corresponding to the region between 0 and 50 ppm. Weak resonances from aromatic cofactors and amino acids appear between 120 and 140 ppm. The signal at 174.5 ppm arises mainly from the buffer. At ~210 ppm, a feature of the backbone carbonyls appears at higher fields. The dark spectra were obtained at different magnetic fields, 17.6 T (spectrum 2A), 9.4 T (spectrum 2B), and 4.7 T (spectrum 2C). As expected for standard NMR experiments, the best spectral quality is obtained at the highest field (spectrum 2A), while several signals are not resolved at 4.7 T (spectrum 2C). The ^{13}C photo-CIDNP MAS NMR spectra obtained under continuous illumination (Figure 3) show both strong negative and positive signals between 80 and 200 ppm. These spectra were recorded at three different magnetic fields, at 17.6 T (spectrum 3A), 9.4 T (spectrum 3B), and 4.7 T (spectrum 3C). The strongest photo-CIDNP effect is observed at 4.7 T (spectrum 3C), while at higher fields, the effect is weakened. Using the broad dark signal at 30 ppm as an internal standard, the photo-CIDNP intensity at 9.4 T is a factor of 3 higher than that at 17.6 T, and at 4.7 T, the relative photo-CIDNP intensity further increases by a factor of 10 relative to the effect at 17.6 T. The same field dependence of the enhancement has been observed in bacterial RCs of *Rb. sphaeroides* WT and R26 (*22, 23*) and PSII (*36*). In contrast, the field dependence of the photo-CIDNP effect in PSI shows a maximum strength at 9.4 T (*36*). In addition, the signal enhancement observed in the light-induced signals from *Hba. mobilis* is unexpectedly strong, considering that the spectra are obtained from unlabeled RCs in membrane fragments.

At high fields, the photo-CIDNP effect in the sample of *Hba. mobilis* is entirely negative (spectrum 3A) which was also observed for RCs of *Rb. sphaeroides* WT (*22*) and PSI (*25*). At 9.4 and 4.7 T, however, this entirely negative signal envelope is changed into a mixed positive and negative pattern (spectra 3B and 3C). Mixed positive and negative patterns are also observed in RCs of *Rb. sphaeroides* R26 (*23*) and PSII (*24*) at all three fields. In these systems, positive signals originate from the donor while negative signals arise from the acceptor. Figure 4 shows the aromatic and carbonylic regions of the light-induced spectra on an expanded scale. Except the signals labeled with an asterisk, all other signals are due to the solid-state photo-CIDNP effect. Due to the strongest photo-CIDNP effect, the best signal-to-noise ratio is observed in spectrum 4C. At high fields (spectrum 4A), the set of positive signals disappears or inverts its sign as observed for the three signals at 155.1, 148.9, and 147.7 ppm. Hence, there seems to be an inversion point of the sign of the subset of signals between 9.4 and 17.4 T. Such field-dependent sign change of a subset of signals has not yet been observed in any other system.

Simulations that assume parameters similar to those for *Rb. sphaeroides* RCs indicate that at all fields the TSM contribution is negative for both the donor and acceptor, the DD contribution is negative for the donor and positive for the acceptor, and the DR contribution is positive and applies only to the donor. The origin of the observed field effect on the sign of the solid-state photo-CIDNP effect may thus be attributed to a variation of the relative contributions of these three photo-CIDNP mechanisms at different fields. This variation would then have to be different from the one observed in other RCs, which might be due to a difference in the exchange coupling between donor and acceptor radicals or due to a difference in the field dependence of the electron spin relaxation rate of the donor triplet. As several parameters with respect to photophysics, geometry, and electronic structure are still unknown for this system, we cannot yet draw a firm conclusion about the origin of the effect.

Effect of Selective Isotope Labeling. The BChl *g* molecule (Figure 1A) contains eight ^{13}C-labeled positions, one of which is aliphatic (C-17). In the 8^1-hydroxy-Chl *a* cofactor (Figure 1B), eight positions are also labeled, and among them, two carbons are aliphatic. ^{13}C photo-CIDNP spectra were recorded at 4.7 T (spectrum 5A) and 9.4 T (spectrum 5B). Both spectra exhibit a pattern of positive and negative photo-CIDNP signals which was also observed for unlabeled RCs. At 4.7 T, five strongly positive signals, which are labeled in red, dominate the spectrum, while negative signals are much weaker. When the intensity ratios of positive to negative signals is compared, on average the relative intensity of the positive signals (spectrum 5A) is larger by a factor of 5 than in the unlabeled samples (spectrum 4C), suggesting an effect of the isotope label concentration on the ratio of the contributions of the three photo-CIDNP mechanisms. Due to the increased level of total hyperfine coupling, isotope labeling may affect the intersystem crossing frequency (*37*). This effect might influence the TSM and DD mechanisms in different ways. Significantly, a higher conversion rate increases the donor triplet yield. This in turn leads to an increased positive DR contribution which is consistent with the observed isotope effect on the relative intensity of positive and negative signals.

Since mass spectrometric analysis showed an isotope label concentration of 12% (see the Supporting Information), compared to a natural abundance concentration of 1%, a signal enhancement by a factor of 12 would be expected upon isotope labeling. When the signal intensities of labeled and unlabeled signals are compared (see below), an enhancement factor of 6 upon labeling has been found for both negative and positive signals. This loss may be due to spin diffusion, although we cannot rule out a direct effect of isotope labeling on the spin chemical machinery, as suggested above.

In the unlabeled sample, no photo-CIDNP is observed in the aliphatic region (Figure 3). On the other hand, in the 4-ALA-labeled sample, a signal appears at 52.0 ppm (Figure 5). Hence, we assume that this aliphatic signal is built up

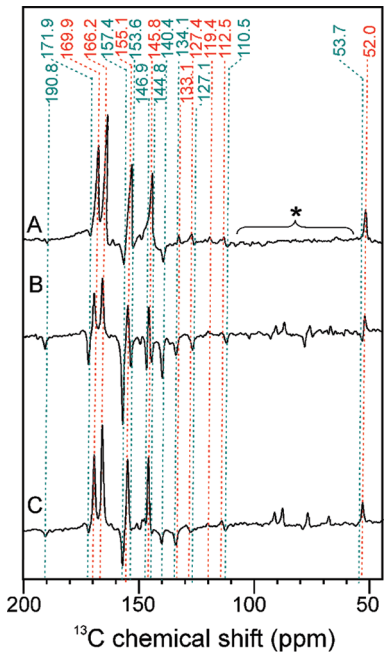

FIGURE 5: ^{13}C photo-CIDNP MAS NMR spectra of 4-ALA ^{13}C-isotope labeled membrane fragments of *Hba. mobilis* obtained under continuous illumination at 4.7 T with a cycle delay of 4 s (A), at 9.4 T with a cycle delay of 4 s (B), and at 9.4 T with a cycle delay of 0.4 s (C). The red color indicates positive signals, while the green color indicates negative signals. In all experiments, the spinning frequency was 8 kHz and the temperature was 240 K. Signals between 100 and 60 ppm marked with an asterisk are spinning sidebands.

by spin diffusion. Similar intensity equilibration of photo-CIDNP signals under the steady-state conditions in an continuous illumination experiment has been observed previously in RCs of *Rb. sphaeroides* WT (*38*). That would imply that the intensities of the aromatic photo-CIDNP signals also have been equilibrated by spin diffusion and the small difference in intensity reflects different local relaxation properties.

Effect of Fast Scanning. Relaxation MAS NMR studies on the RC of *Rb. sphaeroides* WT demonstrate that the T_1 relaxation times of carbon atoms of the donor cofactor are on average 17 s (*21*). All spectra presented until now have been measured at long cycle delays allowing for sufficient relaxation. The unlabeled sample was measured using a cycle delay of 12 s, and for the labeled sample, a 4 s cycle delay has been applied. As shown on various RCs, this difference in cycle delay has no effect on the spectral pattern (*39*). However, the use of very short cycle delays may prevent complete relaxation, and signals of cofactors having a long T_1 may be quenched. Spectrum 5C was recorded at 9.4 T using a high cycle frequency of 0.4 s favoring signals of carbons having a short T_1 relaxation rate. Evidently, the set of negative signals decays dramatically compared to the spectrum measured at the same field with a longer cycle delay (spectrum 5B). As the donor side is generally known to be very rigid (*25, 40*), the relaxation argument would thus indicate that the negative signals arise from donor nuclei. This would imply a different sign of the *g* value difference between donor and acceptor radicals compared to other investigated RCs, which is hardly conceivable. Recently, it has been shown that the activation of the DR allows for fast recovery of the donor signals by enhanced signal recovery

Table 1: Assignment of Absorptive (positive) and Emissive (negative) Photo-CIDNP Signals Observed in Membranes of *Hba. mobilis*[a]

Chl *a*			BChl *a*		*Hba. mobilis*	
σ_{liq}[b]	σ_{ss}[c]	carbon	σ_{liq}[d]	σ_{ss}[d]	positive signals[e]	negative signals[e]
189.3	190.6	13^1	199.3	188.2		190.8
172.7	175.3	17^3	173.4	174.0		
171.0	171.2	13^3	171.6	171.4		
167.4	170.0	19	167.3	168.9	169.9	171.9
161.4	162.0	14	160.8	160.7	162.6	
154.0	155.9	1	151.2	153.5	155.1	157.4
155.8	154.4	6	168.9	170.2	166.2	153.6
151.4	154.0	16	152.2	150.1	151.1	
148.0	150.7	4	150.2	152.2	148.9	
147.7	147.2	11	149.5	147.2	145.0	145.0
146.1	147.2	9	158.5	158.0	147.7	
144.1	146.2	8	55.6			
139.0	137.0	3	137.7	136.1		140.4
135.5	136.1	2	142.1	140.7		
134.2	134.0	12	123.9	119.9		
134.0	133.4	7				
131.5	126.2	13	130.5	124.1	133.1w	134.4
131.5	126.2	3^1	199.3	194.5	127.4w	
118.9	113.4	3^2			119.5w	
107.1	108.2	10	102.4	100.0	110.5w	109.1
106.2	102.8	15	109.7	105.8		102.7
100.0	98.1	5	99.6	98.8		97.6, 96.4
92.8	93.3	20	96.3	93.7		92.1
51.6	51.4	17	50.4		52.0	53.7

[a] Abbreviations: σ, chemical shift; w, weak signals. [b] From ref *42*. The liquid NMR data were obtained in tetrahydrofuran. [c] From ref *43*. The solid-state NMR data were obtained from aggregates. [d] From ref *44*. [e] From this work.

(*39*). Therefore, if the DR mechanism occurs, assignment of the positive signals to the donor would be more reasonable. Occurrence of the DR mechanism would suggest a sufficiently long lifetime of the donor triplet of several microseconds and the absence of triplet quenchers in the direct environment of the donor. We may not safely exclude the possibility that the changes in the spectral pattern are partially due to changes in the relative rate of polarization generation and spin diffusion, which are also caused by the shortening of the cycle delay.

Signal Assignment. The positive signals are best observed at 4.7 T. Upon 4-ALA labeling, the only aliphatic signal appears at 52.0 ppm (spectrum 5A) and can be assigned conveniently to C-17, the only aliphatic ^{13}C-labeled carbon in BChl *g* (Table 1). Such an assignment would imply that the positive signals originate from the donor and are caused by the DR mechanism. If the signal were to originate from the acceptor, two aliphatic signals would be expected, especially due to the hydroxyl group at the 8^1 position; however, there is no indication for signal doubling in the spectrum (spectrum 5A). Hence, we assign the positive signals to the donor side, associating them with BChl *g* (Figure 1A). That would imply that the negative signals originate from the acceptor cofactor, which means that they would be related to a modified plant Chl *a* (Figure 1B).

Upon 4-ALA labeling, four strong signals at 169.9, 166.2, 155.1, and 145.8 ppm appear in the aromatic region (spectrum 5A). Furthermore, four small signals are observed at 133.1, 127.4, 119.5, and 110.5 ppm. Together with the aliphatic signal at 52.0 ppm, which is assigned to C-17, nine positive signals can be identified which arise presumably from the donor.

The chemical shifts of the photosensitive ^{13}C BChl *g* have not yet been reported; however, except for pyrrole ring II,

the chemical composition of the tetrapyrrole ring is identical to that of the well-studied plant Chl *a*. The chemical shift of C-6 may be quite close to that of C-6 in BChl *a*, which is expected at 168.9 ppm (Table 1). The strongest signals appearing at 169.9 and 166.2 ppm can be assigned convincingly to C-19 and C-6, respectively. Since for a Chl *a*, only a single carbon is expected at such high parts per million values, the assignment of the positive signals to the BChl *g* donor is without a plausible alternative. The signals at 155.1 and 145.8 ppm can be attributed to C-1 and C-11, respectively. Labeled C-13 may be assigned to the weak signal at 133.1 ppm. The other three small positive signals arise from unlabeled positions. The signals at 127.4, 119.5, and 110.5 ppm may be assigned to C-3^1, C-3^2, and C-10, respectively. On the other hand, all four weak signals also could conveniently be assigned to histidines (*40*). Recently, involvement of histidines has been observed in PSII (*27*). There is no hint of a positive signal from C-3 and C-8. At such low ^{13}C isotope label concentrations, spin diffusion does not significantly affect the intensities. Since the observed intensities are related to the local electron spin densities, we conclude that on these carbons the electron spin density is low.

In unlabeled samples, nine positive signals are observed at 169.9, 166.2, 162.6, 155.1, 151.1, 148.9, 147.7, 120.4, and 114.2 ppm (spectrum 4C). The signal at 162.6 ppm is conveniently assigned to C-14 and the signal at 151.1 ppm to C-16. The signals at 148.9 and 147.7 ppm match C-4 and C-9, respectively. The signals at 120.4 and 114.2 ppm are in the range of the histidine resonances. Since they appear with a signal intensity similar to those of the unlabeled BChl *g* carbons, their appearance in the spectrum of the 4-ALA-labeled sample is reasonable.

In the 4-ALA-labeled sample, the negative signals are best observed at 9.4 T (spectrum 5B). Signals appear at 190.8, 171.9, 157.4, 153.6, 146.9, 144.8, 140.4, 134.1, 127.1, 112.5, and 53.7 ppm. Assuming that the negative signals originate from the Chl *a* derivative acceptor, the assignment of the signal at 190.8 ppm to the 13^1 carbonyl is straightforward. This signal also has been observed in PSI (*36*) and the RC of *C. tepidum* (*28*); however, it is remarkable that unlabeled carbons show such high intensity. The signal at 171.9 ppm could be assigned to C-19, which is carbon-labeled. The strongest negative signal appears at 157.4 ppm, which matches quite well the labeled C-1 position. The resonance at 153.6 ppm can be attributed to C-6. However, because they are caused by an overlap with the positive signal at 155.0 ppm, the exact positions of the minima may be disturbed. The two negative minima at 146.9 and 144.8 ppm may originate from a single broad negative signal of C-11 overlapping with the positive signal at 145.9 ppm (see below). The signals at 140.4 and 134.1 ppm match the parts per million values expected for labeled C-3 and C-13, respectively. The two signals at 127.1 and 112.5 ppm again may be assigned to histidines (*41*). In the aliphatic region, a negative signal appears at 53.7 ppm and can be assigned to C-8 or C-17. Due to overlap with a positive signal, the exact position is difficult to determine.

For the unlabeled sample, the negative signals are best observed at 4.7 T (spectrum 4C). Five strong signals appear at 190.8, 157.4, 145.0, 134.4, and 112.6 ppm. The signal at 190.8 ppm, which originates from the C-13^1 carbonyl, was even clearly observed in the labeled sample. The resonance at 157.4 ppm was the strongest upon labeling and has been assigned to C-1. Here this signal can be observed without spectral overlap, having an intensity similar to that of the unlabeled carbonyl signal. The C-11 signal appears at 145.0 ppm; hence, the sharp negative features at 146.9 and 144.8 ppm in the spectrum of the labeled compound in fact originate from a single carbon. The signal at 134.1 ppm may be identical with that observed in the labeled sample at 134.4 ppm, which has been assigned to C-13. The signal at 112.6 ppm, which does not change its intensity upon 4-ALA labeling, has been assigned to a histidine. In addition, five weak signals appear in the methine region at 109.1, 102.7, 97.6, 96.4, and 92.1 ppm. Assuming that both signals at 97.6 and 96.4 ppm originate from a C-5, these signals can be conveniently assigned to methine C-10, C-15, C-5, and C-20. The origin of the small splitting of the C-5 signal is not clear. The intensities of the signals of the four methine carbons are roughly similar, suggesting a rather evenly distributed electron spin density at the acceptor.

Since for both positive and negative signals, no signal doubling, with the exception of that of C-5 of the acceptor, is observed in this sample, we conclude that both the donor and primary acceptor are either monomeric or composed of cofactors which are almost identical in their electronic ground states. These findings are in clear contrast to the donor of *Rb. sphaeroides* which shows a double set of signals (*22, 23, 33, 34*) demonstrating the asymmetry of the two halves of the special pair.

Evolutionary Relevance. The solid-state photo-CIDNP effect has been observed in RCs of different groups of photosynthetic organisms. In this paper, we add the heliobacterial RCs to this list, which now contains both types of plant RCs, purple bacterial RCs, green-sulfur bacterial RCs, and heliobacterial RCs. It appears that photo-CIDNP is an intrinsic property of natural RCs, suggesting common structural and kinetic principles. This is remarkable, since the parameter window of the occurrence of this effect has been shown to be very limited (*20*). In addition, the effect appears in RCs from photosynthetic organisms from diverse habitats. On the other hand, despite great effort, photo-CIDNP has not yet been observed in artificial RC systems or other electron transfer systems. Hence, the conditions allowing for the solid-state photo-CIDNP effect seem to be conserved during evolution and may thus be related to functional relevance. The occurrence of the solid-state photo-CIDNP effect may be correlated to the efficient electron transfer in natural photosynthetic systems, since it has not yet been observed, despite great effort, in systems having significantly lower quantum yields. Therefore, the occurrence of photo-CIDNP may provide a guide for optimization of artificial systems.

CONCLUSIONS

Since the solid-state photo-CIDNP effect has now been observed in most of the photosynthetic groups of the evolutionary tree, it appears that the conditions allowing for the effect are conserved in the evolution of RCs and seem to be linked to the high efficiency of light-induced electron transfer in photosynthesis. Photo-CIDNP signals of remarkable intensity have been observed by ^{13}C MAS NMR in the

membrane fragments of *Hba. mobilis*. In analogy to purple bacteria, fast scanning experiments and signal assignment provide evidence that the positive signals originate from the BChl *g* donor. A single complete set of positive signals is detected, demonstrating that the donor is either a monomer or composed of identical cofactors. The negative signals are assigned to the 8^1-hydroxy-Chl *a* acceptor, from which a single set of signals was observed as well. There are strong indications that histidines are carrying electron spin density, probably at both donor and acceptor sides.

ACKNOWLEDGMENT

We thank Mr. A. H. M. de Wit for his expertise in growing the bacteria. The help F. Lefeber, J. G. Hollander, and K. Erkelens in providing technical support is gratefully acknowledged. Prof. H. J. M. de Groot is acknowledged for continuous support. We thank Dr. A. Savitzky for carefully reading the manuscript.

SUPPORTING INFORMATION AVAILABLE

Method for selective isotope label incorporation and determination of isotope label content. This material is available free of charge via the Internet at http://pubs.acs.org.

REFERENCES

1. Neerken, S., and Amesz, J. (2001) The antenna reaction center complex of heliobacteria: Composition, energy conversion and electron transfer. *Biochim. Biophys. Acta 1507*, 278–290.
2. Oh-oka, H. (2007) The antenna reaction center complex of heliobacteria: Composition, energy conversion and electron transfer. *Photochem. Photobiol. 83*, 177–186.
3. Heinnickel, M., and Golbeck, J. H. (2007) Heliobacterial photosynthesis. *Photosynth. Res. 92*, 35–53.
4. Amesz, J. (1995) The Heliobacteria, a new group of photosynthetic bacteria. *J. Photochem. Photobiol., B 30*, 89–96.
5. Brockmann, H., and Lipinski, A. (1983) Bacteriochlorophyll-g: A New bacteriochlorophyll from *Heliobacterium chlorum*. *Arch. Microbiol. 136*, 17–19.
6. Michalski, T. J., Hunt, J. E., Bowman, M. K., Smith, U., Bardeen, K., Gest, H., Norris, J. R., and Katz, J. J. (1987) Bacteriopheophytin-g properties and some speculations on a possible primary role for Bacteriochlorophyll-b and Bacteriochlorophyll-g in the biosynthesis of chlorophylls. *Proc. Natl. Acad. Sci. U.S.A. 84*, 2570–2574.
7. Liebl, U., Nitschke, W., and Mattioli, T. A. (1996) Pigment-protein interactions in the antenna-reaction center complex of *Heliobacillus mobilis*. *Photochem. Photobiol. 64*, 38–45.
8. Trost, J. T., and Blankenship, R. E. (1989) Isolation of a photoactive photosynthetic reaction center core antenna complex from *Heliobacillus mobilis*. *Biochemistry 28*, 9898–9904.
9. Brok, M., Vasmel, H., Horikx, J. T. G., and Hoff, A. J. (1986) Electron-transport components of *Heliobacterium chlorum* investigated by electron paramagnetic resonance spectroscopy at 9 GHz and 35 GHz. *FEBS Lett. 194*, 322–326.
10. Kobayashi, M., van de Meent, E. J., Erkelens, C., Amesz, J., Ikegami, I., and Watanabe, T. (1991) Bacteriochlorophyll-g epimer as a possible reaction center component of heliobacteria. *Biochim. Biophys. Acta 1057*, 89–96.
11. Rautter, J., Bönigk, B., and Lubitz, W. (1996) ENDOR sudies of the cation radical of the primary donor in Heliobacteria suggests that $P798^+$ is a symmetric dimer. *Biophys. J. 70*, A141.
12. Nabedryk, E., Leibl, W., and Breton, J. (1996) FTIR spectroscopy of primary donor photooxidation in Photosystem I, *Heliobacillus mobilis*, and *Chlorobium limicola*. Comparison with purple bacteria. *Photosynth. Res. 48*, 301–308.
13. van de Meent, E. J., Kobayashi, M., Erkelens, C., van Veelen, P. A., Amesz, J., and Watanabe, T. (1991) Identification of 8^1-hydroxy-chlorophyll-a as a functional reaction center pigment in Heliobacteria. *Biochim. Biophys. Acta 1058*, 356–362.
14. Takaichi, S., Inoue, K., Akaike, M., Kobayashi, M., Oh-oka, H., and Madigan, M. T. (1997) The major carotenoid in all known species of heliobacteria is the C-30 carotenoid 4,4′-diaponeurosporene, not neurosporene. *Arch. Microbiol. 168*, 277–281.
15. Brettel, K., Leibl, W., and Liebl, U. (1998) Electron transfer in the heliobacterial reaction center: Evidence against a quinone-type electron acceptor functioning analogous to A_1 in photosystem I. *Biochim. Biophys. Acta 1363*, 175–181.
16. Kleinherenbrink, F. A. M., Chiou, H. C., Lobrutto, R., and Blankenship, R. E. (1994) Spectroscopic evidence for the presence of an iron-sulfur center similar to F_X of photosystem-I in *Heliobacillus mobilis*. *Photosynth. Res. 41*, 115–123.
17. Heinnickel, M., Agalarov, R., Svensen, N., Krebs, C., and Golbeck, J. H. (2006) Identification of F_X in the heliobacterial reaction center as a [4Fe-4S] cluster with an $S = 3/2$ ground spin state. *Biochemistry 45*, 6756–6764.
18. Heinnickel, M., Shen, G. Z., and Golbeck, J. H. (2007) Identification and characterization of PshB the dicluster ferridoxin that harbours the terminal electron acceptors F_A and F_B in *Heliobacterium modesticaldum*. *Biochemistry 46*, 2530–2536.
19. Zysmilich, M. G., and McDermott, A. (1994) Photochemically Induced Dynamic Nuclear-Polarization in the Solid-State ^{15}N spectra of reaction centers from photosynthetic bacteria *Rhodobacter sphaeroides* R-26. *J. Am. Chem. Soc. 116*, 8362–8363.
20. Jeschke, G., and Matysik, J. (2003) A reassessment of the origin of photochemically induced dynamic nuclear polarization effects in solids. *Chem. Phys. 294*, 239–255.
21. Daviso, E., Jeschke, G., and Matysik, J. (2008) Photochemically induced dynamic nuclear polarization (Photo-CIDNP) Magic Angle Spinning NMR, in *Biophysical Techniques in Photosynthesis II* (Aartsma, T. J., and Matysik, J., Eds.) pp 385–399, Springer, Dordrecht, The Netherlands.
22. Prakash, S., Alia, Gast, P., de Groot, H. J. M., Jeschke, G., and Matysik, J. (2005) Magnetic field dependence of photo-CIDNP MAS NMR on photosynthetic reaction centers of *Rhodobacter sphaeroides* WT. *J. Am. Chem. Soc. 127*, 14290–14298.
23. Prakash, S., Alia, Gast, P., de Groot, H. J. M., Matysik, J., and Jeschke, G. (2006) Photo-CIDNP MAS NMR in intact cells of *Rhodobacter sphaeroides* R26: Molecular and atomic resolution at nanomolar concentration. *J. Am. Chem. Soc. 128*, 12794–12799.
24. Matysik, J., Alia, Gast, P., van Gorkom, H. J., Hoff, A. J., and de Groot, H. J. M. (2000) Photochemically induced nuclear spin polarization in reaction centers of photosystem II observed by C-13-solid-state NMR reveals a strongly asymmetric electronic structure of the $P\text{-}680^{\bullet+}$ primary donor chlorophyll. *Proc. Natl. Acad. Sci. U.S.A. 97*, 9865–9870.
25. Alia, Roy, E., Gast, P., van Gorkom, H. J., de Groot, H. J. M., Jeschke, G., and Matysik, J. (2004) Photochemically induced dynamic nuclear polarization in photosystem I of plants observed by ^{13}C magic-angle spinning NMR. *J. Am. Chem. Soc. 126*, 12819–12826.
26. Diller, A., Alia, Roy, E., Gast, P., van Gorkom, H. J., Zaanen, J., de Groot, H. J. M., Glaubitz, C., and Matysik, J. (2005) Photo-CIDNP solid-state NMR on photosystems I and II: What makes P680 special? *Photosynth. Res. 84*, 303–308.
27. Diller, A., Roy, E., Gast, P., van Gorkom, H. J., Glaubitz, C., Jeschke, G., Matysik, J., and Alia, A. (2007) ^{15}N-photo-CIDNP MAS NMR analysis of the electron donor of photosystem II. *Proc. Natl. Acad. Sci. U.S.A. 104*, 12843–12848.
28. Roy, E., Alia, Gast, P., van Gorkom, H. J., de Groot, H. J. M., Jeschke, G., and Matysik, J. (2007) Photochemically induced dynamic nuclear polarization in the reaction center of the green sulphur bacterium *Chlorobium tepidum* observed by ^{13}C MAS NMR. *Biochim. Biophys. Acta 1767*, 610–615.
29. Prakash, S., Alia, Gast, P., Jeschke, G., de Groot, H. J. M., and Matysik, J. (2003) Photochemically induced dynamic nuclear polarisation in entire bacterial photosynthetic units observed by ^{13}C magic-angle spinning NMR. *J. Mol. Struct. 661*, 625–633.
30. Jeschke, G. (1998) A new mechanism for chemically induced dynamic nuclear polarization in the solid state. *J. Am. Chem. Soc. 120*, 4425–4429.
31. Polenova, T., and McDermott, A. E. (1999) A coherent mixing mechanism explains the photoinduced nuclear polarization in photosynthetic reaction centers. *J. Phys. Chem. B 103*, 535–548.
32. McDermott, A., Zysmilich, M. G., and Polenova, T. (1998) Solid state NMR studies of photoinduced polarization in photosynthetic reaction centers: Mechanism and simulations. *Solid State Nucl. Magn. Reson. 11*, 21–47.
33. Schulten, E. A. M., Matysik, J., Alia, Kiihne, S., Raap, J., Lugtenburg, J., Gast, P., Hoff, A. J., and de Groot, H. J. M. (2002) ^{13}C MAS NMR and photo-CIDNP reveal a pronounced asymmetry

in the electronic ground state of the special pair of *Rhodobacter sphaeroides* reaction centers. *Biochemistry 41*, 8708–8717.

34. Prakash, S., Alia, A., Gast, P., de Groot, H. J. M., Jeschke, G., and Matysik, J. (2007) ^{13}C chemical shift map of the active cofactors in photosynthetic reaction centers of *Rhodobacter sphaeroides* revealed by photo-CIDNP MAS NMR. *Biochemistry 46*, 8953–8960.
35. van de Meent, E. J., Kleinherenbrink, F. A. M., and Amesz, J. (1990) Purification and properties of an antenna-reaction center complex from Heliobacteria. *Biochim. Biophys. Acta 1015*, 223–230.
36. Roy, E., Diller, A., Alia, Gast, P., van Gorkom, H. J., de Groot, H. J. M., Jeschke, G., and Matysik, J. (2007) Magnetic field dependence of ^{13}C photo-CIDNP MAS NMR in plant photosystem I and II. *Appl. Magn. Reson. 31*, 193–204.
37. Buchachenko, A. L. (1995) MIE versus CIE: Comparative analysis of magnetic and classical isotope effects. *Chem. Rev. 95*, 2507–2528.
38. Matysik, J., Schulten, E. A. M., Alia, Gast, P., Raap, J., Lugtenburg, J., Hoff, A. J., and de Groot, H. J. M. (2001) Photo-CIDNP C-13 magic angle spinning NMR on bacterial reaction centres: Exploring the electronic structure of the special pair and its surroundings. *Biol. Chem. 382*, 1271–1276.
39. Diller, A., Prakash, S., Alia, Gast, P., Jeschke, G., and Matysik, J. (2007) Signals in solid-state photochemically induced nuclear polarisation recover faster than with the longitudinal relaxation time. *J. Phys. Chem. B 111*, 10606–10614.
40. Fischer, M. R., de Groot, H. J. M., Raap, J., Winkel, C., Hoff, A. J., and Lugtenburg, J. (1992) C-13 Magic angle spinning NMR study of the light-induced and temperature-dependent changes in *Rhodobacter sphaeroides* R26 reaction centers enriched in [4′-C-13]tyrosine. *Biochemistry 31*, 11038–11049.
41. Alia, Matysik, J., Soede-Huijbregts, C., Baldus, M., Raap, J., Lugtenburg, J., Gast, P., van Gorkom, H. J., Hoff, A. J., and de Groot, H. J. M. (2001) Ultrahigh field MAS NMR dipolar correlation spectroscopy of the histidine residues in light-harvesting complex II from photosynthetic bacteria reveals partial internal charge transfer in the B850/His complex. *J. Am. Chem. Soc. 123*, 4803–4809.
42. Abraham, R. T., and Rowan, A. E. (1991) Nuclear magnetic resonance spectroscopy of chlorophyll, in *Chlorophylls* (Scheer, H., Ed.) pp 797–834, CRC Press, Boca Raton, FL.
43. Boender, G. J. (1996) Ph.D. Thesis, University of Leiden, Leiden, The Netherlands.
44. Matysik, J., Alia, Gast, P., Lugtenburg, J., and de Groot, H. J. M. (2001) Photochemically induced dynamic nuclear polarization observed, in bacterial photosynthetic reaction centers observed by ^{13}C solid state NMR, in *Perspectives on Solid State NMR in Biology* (Kiihne, S., and de Groot, H. J. M., Eds.) pp 215–225, Kluwer, Dordrecht, The Netherlands.

BI800030G